

Journal of Materials Chemistry A

Accepted Manuscript



This is an *Accepted Manuscript*, which has been through the Royal Society of Chemistry peer review process and has been accepted for publication.

Accepted Manuscripts are published online shortly after acceptance, before technical editing, formatting and proof reading. Using this free service, authors can make their results available to the community, in citable form, before we publish the edited article. We will replace this *Accepted Manuscript* with the edited and formatted *Advance Article* as soon as it is available.

You can find more information about *Accepted Manuscripts* in the [Information for Authors](#).

Please note that technical editing may introduce minor changes to the text and/or graphics, which may alter content. The journal's standard [Terms & Conditions](#) and the [Ethical guidelines](#) still apply. In no event shall the Royal Society of Chemistry be held responsible for any errors or omissions in this *Accepted Manuscript* or any consequences arising from the use of any information it contains.

PAPER

Core-shell Structured BaTiO₃@Carbon Hybrid Particles for Polymer Composites with Enhanced Dielectric Performance

Cite this: DOI: 10.1039/x0xx00000x

Y. Feng,^{a,b} W. L. Li,^{*a,c} J. P. Wang,^a J. H. Yin,^b and W. D. Fei^{*a,d}

Received 00th January 2012,

Accepted 00th January 2012

DOI: 10.1039/x0xx00000x

www.rsc.org/

Core-shell structured BaTiO₃@Carbon (BT@C) hybrid particles were fabricated via chemical vapor deposition (CVD). The scanning electron microscope, transmission electron microscope, X-ray diffraction and Raman spectra were carried out to confirm the successful fabrication. In order to research the effect of BT@C hybrid particles on the dielectric performance of polymer composites, the PVDF-HFP/BT@C composites were prepared. With the volume fraction of BT@C increasing, the dielectric constant of composites remarkably increased. The dielectric constant of composite with 30vol% BT@C is 1044 at 1 kHz, which is 118 times larger than that of PVDF-HFP (8.8). The experimental results fit well with the percolation theory. The energy storage density of all composites is larger than that of pure PVDF-HFP. The influence of carbon-shell on the dielectric properties of composites is discussed and analyzed. The enhanced dielectric properties are attributed to the increased interfacial polarization in the carbon-shell. These attractive fabrication method of BT@C and features of PVDF-HFP/BT@C composites suggest that the method proposed herein is a new approach to develop high performance composites.

Introduction

Polymer based composites with high dielectric properties are appreciated for their unique combination of mechanical flexibility and tunable dielectric properties.¹⁻⁸ Owing to the lower dielectric constant, various polymers have been modified or filled by different inorganic fillers to achieve excellent dielectric properties.⁹⁻¹³ In terms of the conductivity of fillers, the inorganic fillers to develop high- ϵ composites can be usually divided into three kinds: the insulator, semi-conductor and conductor.¹⁴⁻¹⁶ The typical fillers mentioned above are BaTiO₃, TiO₂, Ag and so on. Dang etc fabricated barium titanate/polyimide (BaTiO₃/PI) nanocomposite films with high dielectric permittivity (20), high breakdown strength (67 MV/m), and high thermal stability by an in-situ polymerization process;¹⁴ Li etc reported a kind of ferroelectric

polymer with TiO₂ nanoparticles exhibiting significantly enhanced electrical energy density;¹⁵ Qi etc provided an approach to fabricate appropriate epoxy/Ag composites with excellent electrical and mechanical properties, which can be used as embedded capacitors in the printed-circuit-board (PCB) manufacturing methodologies.¹⁶

In terms of the microstructure and dimension, the fillers in the nanocomposites can be also separated into three types: sphere-filler, wire/rod-filler and sheet-filler. The classical examples are ceramic nanoparticles, ceramic nanowire, carbon nanotube, graphene and so on.¹⁷⁻²¹ It is well known that BaTiO₃ or TiO₂ nanowire as filler can increase the dielectric properties of polymer-based composites;¹⁷⁻¹⁹ The variation of dielectric constant in composites filled by carbon nanotube fits well with the percolation theory;²⁰ Graphene as 2-D filler can remarkably reduce the percolation threshold in the polymer composites.²¹

For one kind of filler mentioned above, its effect on the dielectric properties is also limited and sole. Considering the above reason, in developing multifunctional polymer composites, two or more kinds of fillers are doped into polymer matrix to fabricate three or more-phase composites.²²⁻²⁷ Although the enhanced dielectric properties can be easily achieved in three or more-phase composites, the degradation of other properties can't be avoided due to higher volume fraction of inorganic and weak compatibility between inorganic-polymer matrix. Researcher began considering whether the combination of two kinds of fillers with different physical properties, namely hybrid particles can be obtained before filling.^{13, 28, 29} Recently, many studies have been focused on the fabrication of

^a School of Materials Science and Engineering, Harbin Institute of Technology, Harbin 150001, P.R. China

^b Key Laboratory of Engineering Dielectrics and Its Application, Ministry of Education, Harbin University of Science and Technology, Harbin 150080, P. R. China.

^c National Key Laboratory of Science and Technology on Precision Heat Processing of Metals, Harbin Institute of Technology, Harbin 150001, P.R. China. Email: wlli@hit.edu.cn

^d State Key Laboratory of Advanced Welding and Joining, School of Materials Science and Engineering, Harbin Institute of Technology, Harbin 150001, P.R. China. Email: wdfei@hit.edu.cn

hybrid particles: the surface of ceramic particles can be modified by the surfactant adsorptions, polymer coatings or conductive materials coatings. A physical compatibility along with more novel interface can be formed to guarantee good dispersion of the ceramics particles.³⁰⁻³³ Many researchers had reported that the nano-sized Ag particles discretely deposited on the BT surface can efficiently enhance the dielectric permittivity of the BT-Ag/PVDF composite.³⁴ The Ag coating $\text{CaCu}_3\text{Ti}_4\text{O}_{12}$ (CCTO) particles had been fabricated, and their polyimide composites were investigated. The enhancement of dielectric permittivity is attributed to the increment of conductivity of the interlayer between CCTO and PI by Ag.³⁵ In addition, reduced graphene oxide-encapsulated SiO_2 hybrid particles were fabricated and their polymer-based composites possess enhanced thermo-mechanical properties. The special core-shell structure is believed to make full use of the enhancement effect of different components and endow the polymer composites with outstanding properties overall.³⁶ Lots of previous studies demonstrate that conductive materials coatings on the ceramic particles can result in enhanced dielectric properties in the polymer based composites.

Poly(vinylidene fluoride) (PVDF), which is a semicrystalline thermoplastic polymer with remarkable high piezo- and pyroelectric coefficient, excellent thermal stability and chemical resistance, and its derivative copolymers such as poly(vinylidene fluoride-co-trifluoroethylene) [P(VDF-TrFE)], and poly(vinylidene fluoride-co-hexafluoropropylene) [PVDF-HFP] have been employed to fabricate high- ϵ composites. In present study, core-shell structured BT@C hybrid particles were fabricated via chemical vapor deposition. PVDF-HFP/BT@C composites were fabricated to research the effect of hybrid particles on the dielectric performance of polymer based composites. The BT@C hybrid particles were characterized by scanning electron microscopy, transmission electron microscopy, Raman spectroscopy, thermo-gravimetric analysis and the composites were studied by scanning electron microscopy and X-ray diffraction. The dielectric properties and energy storage density of the composites filled by the BT@C were also measured and discussed. Finally, the influence of C-shell on the dielectric performance of composites was analyzed carefully. The BT@C in the composites was found to have significant and interesting influences on the dielectric properties of the composite system.

Experimental

Materials

PVDF-HFP was purchased from Sigma-Aldrich Co. Ltd. BaTiO_3 nanoparticles (BT) were purchased from Aladdin Industrial Corporation with the average size of 100 nm and sieved out prior to use. Carbon-shell coating BaTiO_3 -core hybrid particles (BT@C) were fabricated by CVD, and the preparation process was shown in the Figure 1. Nickel nitrate hexahydrate ($\text{Ni(NO}_3)_2 \cdot 6\text{H}_2\text{O}$) and methyl alcohol were purchased from Shanghai Chemical Corp. All other chemicals were obtained as analytical grade products and used without further purification.

Preparation of BT@C hybrid particles

In this process, 1.5 g $\text{Ni(NO}_3)_2 \cdot 6\text{H}_2\text{O}$ was dissolved into methyl alcohol. 8.5 g BT was then added with fast stirring.³³ The mixture

was stirred vigorously for 60 min and then heated at 100 °C for 6 h to remove methyl alcohol, which was subsequently cooled to room temperature. The products were $\text{BaTiO}_3 @ \text{Ni(NO}_3)_2 \cdot 6\text{H}_2\text{O}$. In order to fabricate the C-shell around the BaTiO_3 particles, the $\text{BaTiO}_3 @ \text{Ni(NO}_3)_2 \cdot 6\text{H}_2\text{O}$ were placed at the centre position of a quartz tube reactor heated to about 800 °C under flowing argon/hydrogen (10:1 molar ratio) gas mixture. Under the high temperature circumstance, the $\text{Ni(NO}_3)_2 \cdot 6\text{H}_2\text{O}$ will be broken down as following reaction equation:



When the hydrogen is passed through the quartz tube, the NiO can be reduced into Ni. Ni is usually used to be the catalyst for the fabrication of carbon and its derivatives.^{37, 38} After reaching to the desired temperature (800 °C), a flow of methane (CH_4) gas was introduced into the reactor with a rate of 20 Sccm for about 30 min. A black coating covered the surface of the nanoparticles is C-shell. Then quartz tube reactor was subsequently cooled to room temperature. The black powder is BT@C hybrid particles. Major technology parameters in this preparation are listed in Table 1.

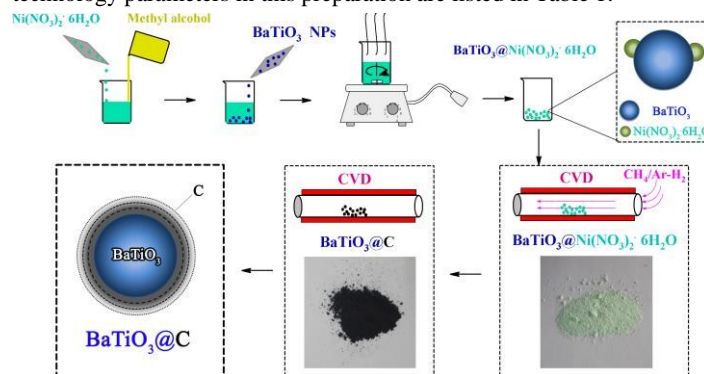


Figure 1. Synthesis of BT@C hybrid particles

Preparation of PVDF-HFP composites

The PVDF-HFP/BT@C composites were prepared by employing solution blend. The as-synthesized BT@C particles were ultrasonically dispersed in N, N-Dimethylformamide (DMF) for 0.5 h. Then PVDF-HFP was added into the system with mechanical stirring for 2 h at 70 °C. Then the mixture was casted on clean glass plates and dried at 120 °C for 2 h in an oven. The prepared composites filled by various volume fraction and thickness of 25-35 μm were collected for test.

Table 1. Technology parameters in fabrication of BT@C hybrid particles

	Pressure	Catalyst	Temperature	Gas	Time
BT@C	Ordinary pressure	Ni	800 °C	$\text{CH}_4/\text{H}_2\text{-Ar}$ 20/80	30 min

Characterization

The scanning electron microscope (SEM) observation was performed on a Helios Nanolab 600i. The transmission electron microscope (TEM) observation was performed on a Tecnai F30. The wide-angle X-ray diffraction (XRD) experiment was performed on a Philips X'Pert diffractometer with $\text{CuK}\alpha$ radiation generated at 40 kV and 40 mA. Raman spectra were carried out using a micro-Raman Renishaw spectrometer. The laser line (514 nm) was used to excite the sample. Thermo-gravimetric

analysis (TGA) was performed using TGA/SDTA851E thermogravimetric analyzer at a heating rate of 10 °C/min in air. Prior to dielectric measurements, Ag electrodes were deposited onto both surfaces of the specimens by sputtering. The dielectric spectroscopy and conductivity were carried out using an impedance analyzer (Agilent 4294A) in the frequency range of 10^2 to 10^6 Hz. The relative humidity ($\approx 50\%$) of the measurement environment remained constant throughout the investigation and temperature varied in the range of 30-120 °C. The polarization-electric field (P - E) hysteresis loops were determined using a Radiant Technologies Precision work station. Tensile tests were performed on a tensile test machine (Instru-Met Corp.). The samples were loaded in constant deformation mode at a speed of 5 mm/min. Three samples were used for each test.

Results and Discussions

Characterization of BT@C hybrid particles

SEM and TEM measurements were employed to identify the morphology of the BT@C hybrid particles (Fig. 2). Fig. 2(a) and (b) are the SEM images of pure BT and BT@C particles, respectively. Compared with the pure BT particles, after high-temperature treatment, there is little change in the size of BT@C. The size of BT@C particles is still in the range of 70-120 nm. TEM image of BT@C and high resolution TEM (HRTEM) image of interfacial microstructures are displayed in Fig. 2(c) and (d), respectively. The observation in Fig. 2(c) can be used to distinguish clearly the BT-core and C-shell through different gray scale, which indicates that the C-shell are coating the BT-core. As shown in Fig. 2(c), it is clear that the C-shell with a thickness of 5-15 nm. Fig. 2(d) shows the high resolution TEM image in the solid line square of Fig 2(c). Fig. 2(d) confirms that the combination between BT-core and C-shell is strong, and no phase separation exists.

XRD pattern of the as-synthesized BT@C hybrid particles is given in Fig. 3(a). All the diffraction peaks can be assigned to the tetragonal phase of BT without any impurity, in good agreement with the reported data (JCPDS, 81-2203).³⁹ It is clearly seen that the crystal structure of BT-core isn't changed during the CVD treatment.

The presence of C-shell was confirmed by Raman spectroscopy, which has been utilized as a powerful tool for the characterization of carbon and its derivatives. Fig. 3(b) shows the Raman spectra of the BT@C hybrid particles. The Raman spectra of carbon are characterized by two main features, the peak at 1574 cm^{-1} is a so-called G-band, and those at 1340 cm^{-1} are D-band. The G-band referring to graphite comes from the first-order scattering of the E_{2g} phonon of C sp^2 atoms, and the D-band which is associated with a breathing mode of k -point photons of A_{1g} symmetry is observed in the presence of defects.^{40, 41} Therefore, the intensity of D-band is proportional to the amount of disorder (crystallite boundary) in the sample, and the ratio between the intensities of the disorder-induced D-band and the first-order graphite G-band (I_D/I_G) provides a parameter that can be used for quantifying graphitic ordering and disorder. In brief, the lower the I_D/I_G value is, the higher the graphitic

ordering of graphite is. For the carbon and its derivatives fabricated by chemical vapor deposition technique, I_D/I_G value is usually in the range of zero to three.⁴²⁻⁴⁴ Compared with the I_D/I_G values in the previous papers, the value in the present study (0.78) is smaller, which demonstrates that higher quantity C-shell with preferable graphitic ordering is coating BT-core.

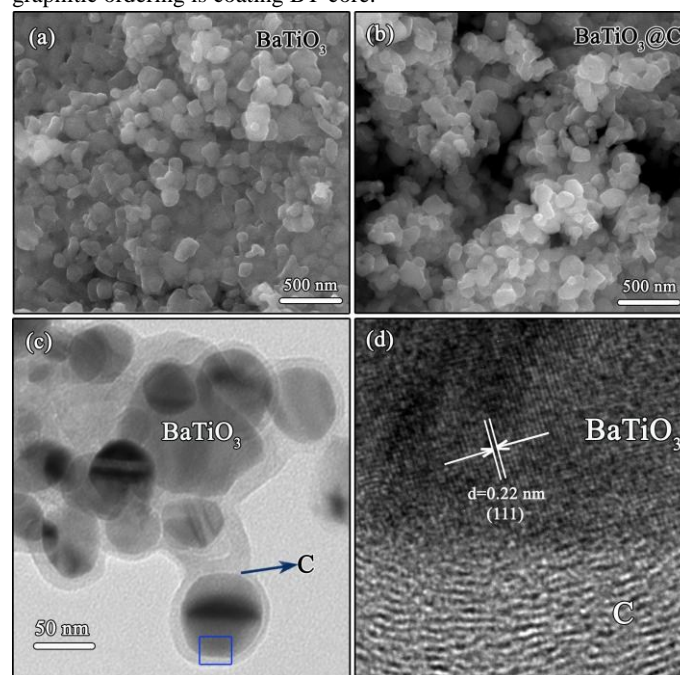


Figure 2. SEM images of (a) BT, (b) BT@C, TEM image of (c) BT@C and (d) is the high resolution TEM image in the solid line square of (c)

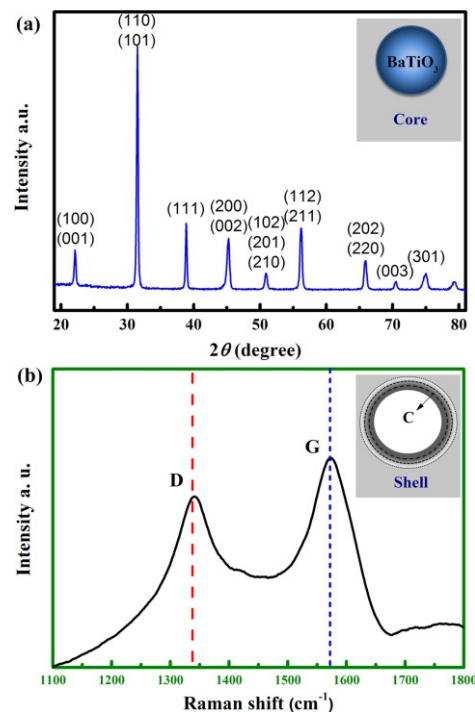


Figure 3. XRD pattern (a) and Raman spectra (b) of BT@C hybrid particles

To get more precise information about BT@C, the TGA curves of the BT@C and BT particles were measured. Fig. 4 shows the weight loss of pure BT and BT@C hybrid particles.

It can be seen from Fig. 4(a) that: on the one hand, weight loss of the particles shows the order of $BT < BT@C$ at 900 °C, namely, the weight loss of the $BT@C$ particles is larger than that of BT; on the other hand, there are remarkable weight loss in the temperature range of 500-700 °C corresponding to the carbon, which indirectly confirms that C-shell is onto the surface of BT-core.⁴⁵ The differences in the TGA data of BT and $BT@C$ not only present further evidence to prove the coating of C-shell around the BT-core, but also obtain approximately the C-shell mass fraction of about 2.5 wt% in the $BT@C$ hybrid particles.

Besides, the conductivity of $BT@C$ is carried out and the result is shown in Fig. 4(b). The conductivity of $BT@C$ is in the range of 10^{-4} - 10^{-2} S/m, namely, $BT@C$ exhibits typical semiconductor characterization. However, it is well known that BT is a kind of excellent insulator. Obviously, this change of conductivity is due to the synthesized C-shell on the BT surface.

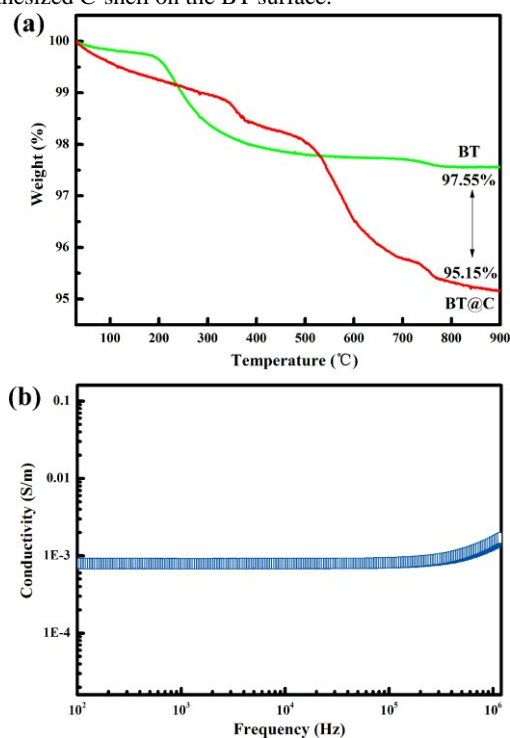


Figure 4. (a) TGA curves of BT and $BT@C$ particles, (b) Conductivity of $BT@C$ hybrid particles

Characterization of Composites

We fabricated two kinds of composites containing $BT@C$ and BT particles, respectively. Fig. 5 shows the XRD patterns of pure PVDF-HFP, PVDF-HFP/BT-0.10 and PVDF-HFP/ $BT@C$ -0.10 composites. The peaks at 18.4°, 20.8° and 26.6° corresponding to the PVDF α -phase, β -phase and γ -phase diffraction, respectively. For two types of composites, the characteristic diffraction peaks of $BaTiO_3$ appear at about $2\theta = 22^\circ, 31^\circ, 38^\circ$, which are associated with typical structure of perovskite BT in crystal planes of (100), (110) and (111).⁴⁶ Because the characteristic of carbon in XRD pattern is not obvious, there is no peak corresponding to C-shell. The XRD patterns of the composites show both BT and PVDF-HFP diffraction peaks, which clearly demonstrates that BT and $BT@C$ are filled in the polymer matrix.

Fig. 6 displays cross-section SEM images of PVDF-HFP/BT@C-0.05 and PVDF-HFP/BT@C-0.20 composites. $BT@C$ particles with sphere-sharp disperse homogeneously into the PVDF-HFP matrix. Moreover, the dispersion of $BT@C$ in the matrix is excellent since there is no obvious aggregation observed in both composites.

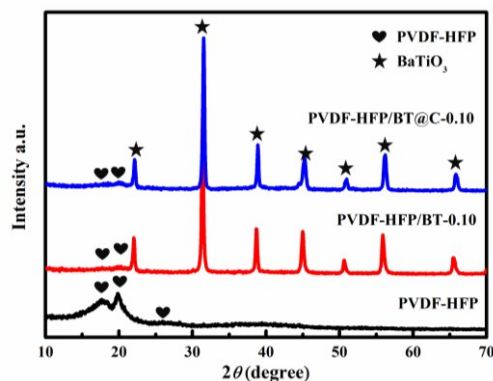


Figure 5. XRD patterns of PVDF-HFP, PVDF-HFP/BT-0.10 and PVDF-HFP/ $BT@C$ -0.10 composites

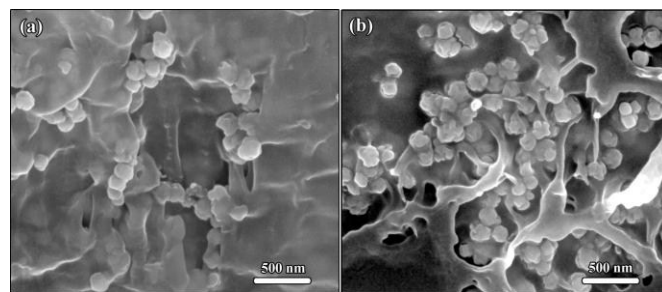


Figure 6. Cross section SEM images of (a) PVDF-HFP/ $BT@C$ -0.05, (b) PVDF-HFP/ $BT@C$ -0.20 composite

Dielectric properties of composites

The dependence of the dielectric constant of composites filled by $BT@C$ on the frequency is shown in Fig. 7(a). With the volume fraction of $BT@C$ increasing, the dielectric constant of the composites increases. When the fraction is less than 10 vol%, the increment of dielectric content is lower (see Fig. 7(a) inset). When the fraction is greater than 10 vol%, however, the increment of dielectric content is large (see Fig. 7(a)). Dielectric constant of composites exhibits gradually increased frequency dependence as the volume fraction increasing, especially at lower frequency. For comparison, the dielectric constant of composites filled by BT is also measured and shown in Fig. 7(b). Dielectric constant of the composites also increases with the volume fraction of BT particles. The effect of BT particles on the dielectric constant of composites is similar to $BT@C$ particles. As the ceramic fillers have a much larger dielectric constant, most of the increment in effective dielectric constant of the composites comes from the increase in the average field in the polymer matrix. The similar result has been reported in other composite systems.^{14, 30} However, the enhanced effect of $BT@C$ on dielectric constant at lower frequency is far larger than that of BT particles. Dielectric constant in PVDF-HFP/ $BT@C$ composites exhibits stronger frequency dependence than that's in PVDF-HFP/BT composites. The trend of dielectric constant in PVDF-HFP/ $BT@C$ composite confirms that the enhanced effective

dielectric constant is not just the result from the contribution of average field.

It is worth mentioning that there is a few Ni catalyst left in the hybrid particles. In order to confirm the improvement of dielectric properties stemmed from the C-shell rather than Ni, the PVDF-HFP/BT@Ni composites were prepared for the dielectric properties test after the NiO was reduced into Ni. The dependence of the dielectric constant of composites filled by BT@Ni on the frequency is shown in Fig. 7(c). There is obviously enhanced effect of BT@Ni on the dielectric constant of composites. By comparing the PVDF-HFP/BT@Ni and PVDF-HFP/BT composites with same loading, the dielectric constant of PVDF-HFP/BT@Ni composite is larger than that of PVDF-HFP/BT composite. However, the dielectric constant of PVDF-HFP/BT@Ni-0.20 and -0.30 composites is still far smaller than that of PVDF-HFP/BT@C-0/20 and -0.30 composites, respectively. The variation of dielectric constant in PVDF-HFP/BT@Ni composites at lower frequency is also different from that in PVDF-HFP/BT@C composites. The above mentioned comparison indicates that the increment in dielectric constant of PVDF-HFP/BT@C composites should be attributed to the synthesized C-shell rather than Ni.

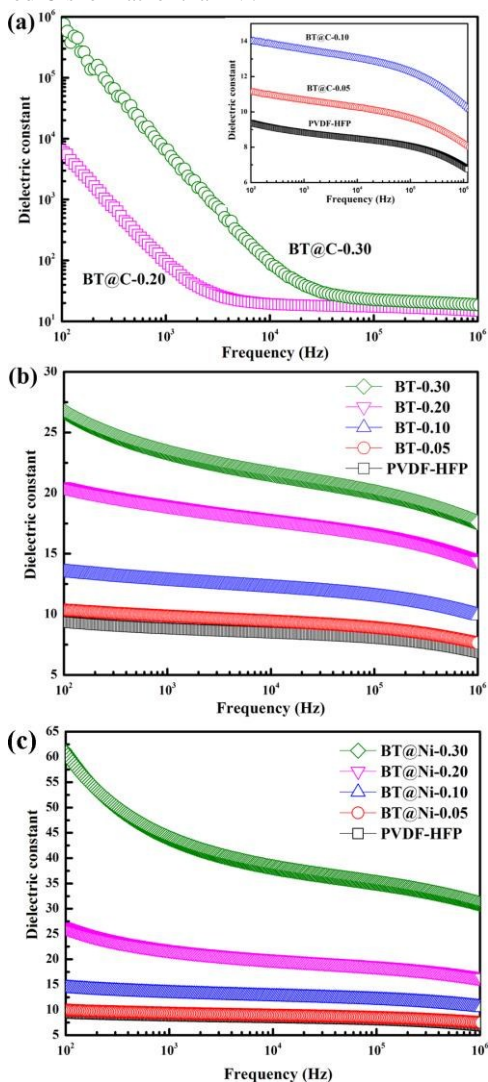


Figure 7. Dependence of dielectric constant of PVDF-HFP/BT@C (a), PVDF-HFP/BT (b) and PVDF-HFP/BT@Ni (c) composites on the frequency

The variation of dielectric constant in the composites with BT@C and BT particles at 1 kHz are shown in Fig. 8(a). It can be seen that, the dielectric constant of 20 vol% PVDF-HFP/BT@C composite is above 88, which is 4 and 10 times larger than that of the composites filled by 20 vol% BT (19.4) and pure PVDF-HFP (8.8), respectively. Meanwhile, dielectric constant in 30 vol% PVDF-HFP/BT@C composite is above 1044, which is 45 and 118 times larger than that of the composites filled by 30 vol% BT (23) and pure PVDF-HFP, respectively. This enhanced effect of BT@C on the dielectric constant can't be understood by enjoying the classical theory and models, for instance Maxwell-Garnett model, Logarithmic model or EMT model.^{47, 48}

Fig. 8(b) shows loss tangent as a function of frequency for PVDF-HFP/BT@C composites. With the frequency increasing, loss tangent of composites decreases. Meanwhile, loss tangent increase with the volume fraction increasing. The loss tangent of PVDF-HFP/BT@C is 0.028 at $f=0.05$ and 0.025 at $f=0.10$. In the case of $f \geq 0.20$, a dramatic increment of loss tangent ($f=0.20$: 1.9 and $f=0.30$: 17) along with dielectric constant appears. It is possibly resulted from following reason. In addition to the monodispersed BT particles encapsulated by C-shell, there should be a few clusters of BT particles encapsulated by C-shell existing in the hybrid particles. The clusters doubtlessly increase the volume of connected C-shell on the BT surface (similar to local agglomeration). The C-shell possessing excellent conductivity can produce electrical current under electrical field. The electrical current can possibly transmit in the connected C-shell, and part of electrical energy will transfer into thermal energy. The higher the volume of connected C-shell is, the larger the thermal energy is. With the volume fraction of filler increasing, there is more and more C-shell connecting with each other. Thus, there is higher dielectric loss observed in the PVDF-HFP/BT@C-0.20 and -0.30 composites.²⁸

In order to research the insulation of composites, the conductivity of composites with BT@C hybrid particles is measured and the results are shown in Fig. 8(c) and (d). As $f \leq 0.10$, the conductivity shows strong dependence of frequency because of the insulating nature. The conductivity increases with the frequency on the basis of an apparent power law: $\sigma(\omega) = \omega^n$ ($0.6 \leq n \leq 1$).⁴⁹ With a further increment of the volume fraction to 0.30, an obvious insulator-semiconductor transition is observed, which indicates the formation of conductive paths in the composite.

An excellent property of a dielectric material is not only its ability to increase capacitance, but also, and equally important, its mechanical performance. The tensile strengths of the PVDF-HFP/BT@C composites are carried out, and the results are shown in Fig. 8(e). With the volume fraction of fillers increasing from 0 vol% to 30 vol%, the tensile strength of PVDF-HFP/BT@C composites decreases from 31.17 to 23.48 MPa. The hybrid particles weaken the mechanical performance of composites owing to the influence of fillers on the matrix structure. Although the tensile strength exhibits slight downtrend with the volume fraction of BT@C increasing, it still meets the specification and operating requirement.

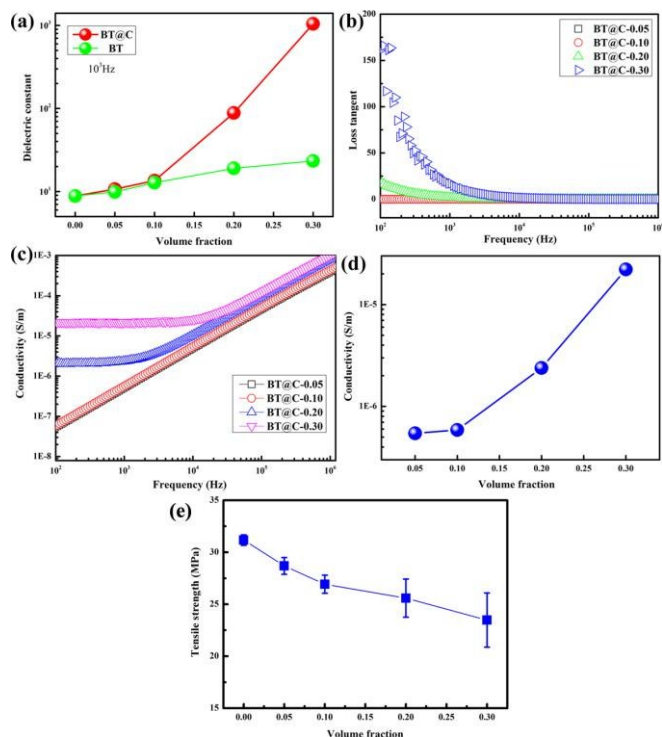


Figure 8. (a) Dielectric constant of composites as a function of volume fraction at 1 kHz, Dependence of loss tangent (b) and conductivity (c) on the frequency, (d) Conductivity of composites as a function of volume fraction at 1 kHz and (e) tensile strength of composites as a function of volume fraction

It could be observed that a limited increment in the dielectric constant and conductivity occurred when $f \leq 10$ vol%, and then a sudden large increase appeared when $f \geq 10$ vol%. Percolation theory, which is considered as a typical theory in polymer composites with conductive fillers, can be employed to explain this phenomenon.^{50, 51} The dielectric constant of PVDF-HFP/BT@C composites near the percolation threshold can be described by equation (2) as follows:

$$\varepsilon_{\text{eff}} \propto \varepsilon_b (f_c - f)^{-s} \quad (2)$$

Where ε_b is the dielectric constant of the PVDF-HFP matrix, f is the volume fraction of BT@C particles, f_c is the percolation threshold of composites, and s denotes a critical exponent in the insulating region. Fig. 9 shows that the experimental results fit well with percolation theory (the fitting parameters f_c and s are 0.28 and 1.923, respectively). The linear fit of the log value of dielectric constant and volume fraction also indicates that the dielectric constant fits well with percolation theory (see Fig. 9 inset). The universal value of the percolation threshold f_c is in the range of 0.3-0.6 for two-phase random media.⁵² The decreasing of the percolation threshold (0.28) in present research should be attributed to the conductive C-shell on the BT surface. With the volume fraction increasing, the distance between the neighbouring BT@C particles is reduced. The conductive network is easily formed because of the conductive C-shell. The dielectric constant of composites will be enhanced due to the percolation effect. Owing to the outstanding conductivity of C-shell and the formation of electrical paths in the PVDF-HFP matrix, the dielectric loss and conductivity also increase near the percolation threshold.

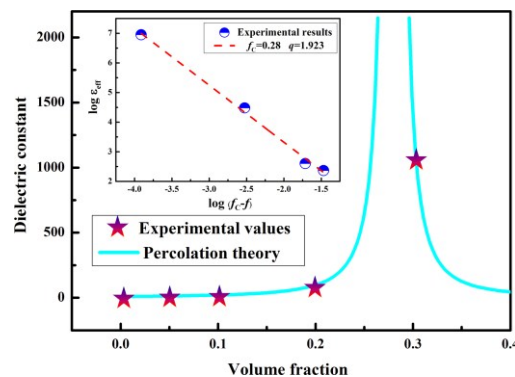


Figure 9. Comparison of experimental and theoretical dielectric constant as a function of the volume fraction

Energy storage density of composites

For the ferroelectrics, because the polarization is not linearly dependent on the electric field, the energy storage density should be calculated from the P - E loops for PVDF-HFP composites.⁵³ The unipolar P - E loops for composites with different fraction of BT@C are measured at 10 Hz. The P - E loops are shown in Fig. 10(a). The maximum and remnant polarization of composites loaded with various fraction are greater than those of pure PVDF-HFP. For instance, the maximum polarization of the composites with BT@C-0.30 is 2.15 $\mu\text{C}/\text{cm}^2$ at 1400 kV/cm , which is 2.4 times higher than that of the pure PVDF-HFP (0.89 $\mu\text{C}/\text{cm}^2$). Since the dielectric constant of BT is much bigger, the distribution of electric field is distorted, which leads to higher electric field in the matrix and larger polarization of the matrix. In addition, the BT particles as a kind of ceramic particles with high dielectric constant will increase the statistical polarization of composites under the applied electric field.

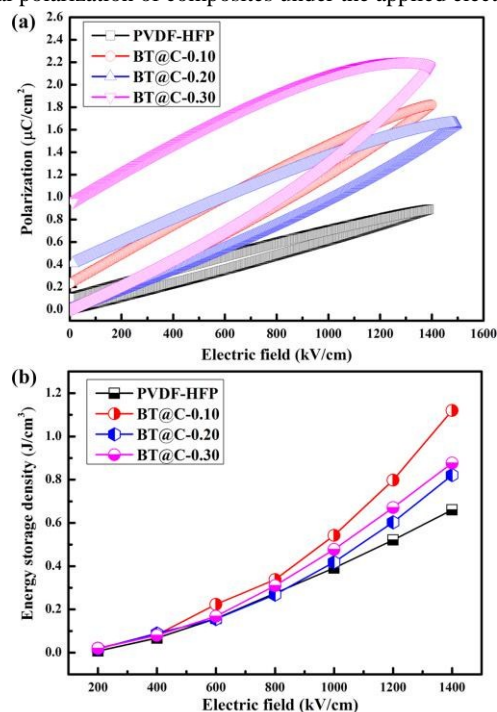


Figure 10. The unipolar P - E loops (a) and energy storage density (b) of PVDF-HFP/BT@C composites with different fraction at 10 Hz

The energy storage density is calculated according to the formula $U = \int E dD$.¹⁹ The energy storage density of composites with various fraction as function of electric field is shown in Fig. 10(b). With the electric field increasing, the energy storage density of all samples is enhanced obviously. The uptrend of energy storage density for composites is more obvious than that for pure PVDF-HFP. The maximal energy storage density of 1.1 J/cm³ is obtained at 1400 kV/cm in composites with 10 vol% BT@C particles, which is 38% bigger than that of the pure PVDF-HFP (0.8 J/cm³). There are leakage phenomenon and unsaturated loops observed in PVDF-HFP/BT@C-0.20 and 0.30 composites, which result in the lower energy storage density. Thus, the results demonstrate that more does not necessarily mean better, and there is a certain volume fraction for the best performance.

Carbon-shell and enhanced dielectric performance

A multicore model has been put forward to describe the interfacial areas of nanocomposites, which shows that the Gouy–Chapman diffuse layer exists and results in charge accumulation at the interface areas.^{54, 55} Fig. 11(a) shows the model and charge distribution of Gouy–Chapman diffuse layer in polymer–filler interface. The diffuse layer is regarded as a significant factor on the interfacial polarization in the polymer-based composites. For the PVDF-HFP/BT composites, the diffuse layer is located in the polymer matrix. For the PVDF-HFP/BT@C composites, the diffuse layer will exist in the C-shell, which acts as the interfacial area between PVDF-HFP matrix and BT. It is easy for charge to exist in the C-shell compared with polymer matrix. C-shell will undoubtedly provide the condition for the charge. The occurrence of charge accumulation in diffuse layer will result in enhanced interfacial polarization and dielectric response under electric field.

To further demonstrate that large interfacial polarization existing in the PVDF-HFP/BT@C composites, the activation energy (E_a) of the composites was calculated. According to the Arrhenius law the conductivity (σ) is strongly dependent on temperature (T), and the equation can be written as:

$$\sigma(T) = \sigma_0 \exp\left(-\frac{E_a}{kT}\right) \quad (3)$$

where σ_0 is a pre-exponential term and represents the high temperature limit of conductivity, while k and T are the Boltzmann constant and the absolute temperature, respectively. The E_a can be obtained from the plots of $\ln\sigma$ versus $1000/T$.^{56, 57}

Fig. 11(b) shows the dependence of $\ln\sigma$ on $1000/T$ at 100 Hz for the pure PVDF-HFP, PVDF-HFP/BT@C-0.10, PVDF-HFP/BT@C-0.20 and PVDF-HFP/BT@C-0.30 composites, respectively. It is clearly seen that the curves of pure PVDF-HFP and PVDF-HFP/BT@C-0.10 composite over the whole range could be fitted to straight line. The calculated E_a of them is 0.520 eV and 0.085 eV, respectively. The E_a of PVDF-HFP is reduced due to the incorporation of BT@C. Meanwhile, the E_a of PVDF-HFP and PVDF-HFP/BT-0.10 composites is both positive. The positive activation energy implies that the movement of electrons is restricted and the free charges available at the interface move difficultly when an electric field is applied. However, the E_a of PVDF-HFP/BT@C-0.20 and PVDF-HFP/BT@C-0.30 composites is different from above two. For the PVDF-HFP/BT@C-0.20 composite, negative E_a

($E_a = -0.239$ eV) and positive E_a ($E_a = 0.114$ eV) are found in the range of lower and higher temperature, respectively. When the fraction is added further to 0.30, the E_a present only positive value ($E_a = -0.207$ eV) in the range of 30–120 °C. The appearance of negative activation energy indicates that a large number of electrons are possible present at the interface of the PVDF-HFP/BT@C composites, then results in higher conductivity and strong interfacial polarization. The variation of E_a is confirmed to be associated with volume fraction of BT@C. With the volume fraction increasing, the E_a possesses a change from positive to negative value.

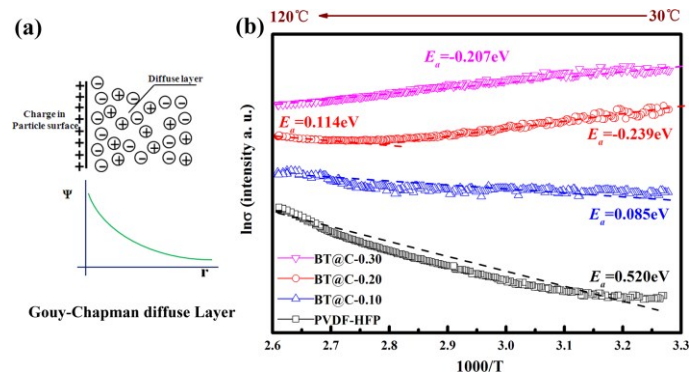


Figure 11. (a) Charge distribution in Gouy–Chapman diffuse layer and (b) Dependence of $\ln\sigma$ on $1000/T$ for the PVDF-HFP and PVDF-HFP/BT@C composites with different volume fraction

In view of the previous data on dielectric loss and conductivity, we find that the dielectric properties of PVDF-HFP/BT@C-0.20 and 0.30 composites are similar to that of PVDF/conductive fillers: higher dielectric loss, conductivity, and negative E_a . It is possibly resulted from following reason: the C-shell is a kind of conductive materials. There should be a few charge carriers existing in the C-shell which is located between the BT-core and PVDF-HFP matrix. Under electric field or thermal excitation, it is easy for the charge carriers to transfer. The characters of carriers in the C-shell are similar to that in the conductive fillers. Considering the low weight percentage of C-shell in hybrid particles, the only difference is that the concentration of carriers in the C-shell is lower than that in conductive fillers.

When the temperature is lower, the carriers in the C-shell of PVDF-HFP/BT@C-0.02 composite can be easily excited and participate in conduction and interfacial polarization, thus E_a in the PVDF-HFP/BT@C-0.20 composite is negative and dielectric constant is enhanced remarkably. With the temperature increasing, no more carriers can be excited and take part in the conduction, so E_a becomes positive again. In the same way, the E_a of the PVDF-HFP/BT@C-0.30 composite is negative in the measured temperature range because more carriers than that in PVDF-HFP/BT@C-0.20 composite can participate in the conduction and interfacial polarization. Thus, higher dielectric constant, dielectric loss, conductivity and negative E_a are observed in PVDF-HFP/BT@C-0.20 and 0.30 composites. The experimental results confirm what we expected. The improvement of dielectric constant in PVDF-HFP/BT@C composites is attributed to the enhancement of interfacial polarization.

The average inter-filler distance between neighbouring particles for PVDF-HFP/BT@C composites can be calculated using the

relation: $d = r \times (4\pi/3f)^{1/3}$ where f is the volume fraction of fillers and r is the average radius of the BT particles.⁵⁸ For the composites with 10 vol% BT@C (Fig. 12(a)), d is in the range of 160-180 nm. Considering the width of C-shell (5-15 nm), nevertheless, there are so far instance between the surfaces of neighbouring particles. For the composites with 30 vol% BT@C (Fig. 12(b)), the d is reduced to 110-130 nm. Assuming that the radius of BT particles is in the range of 70-120 nm, the neighbouring diffuse layers or C-shell possibly overlap. Thus, the space charge can transfer across the neighbouring C-shell and the conductivity and dielectric loss increase largely. The above analysis confirms what we discuss about the dielectric loss and conductivity near percolation threshold again.

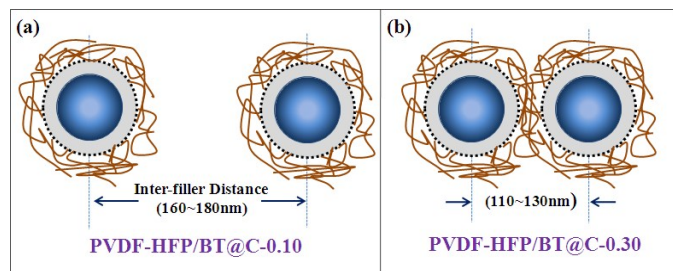


Figure 12. Diagrams of neighbouring particles in PVDF-HFP/BT@C-0.10 (a) and PVDF-HFP/BT@C-0.30 (b)

Conclusions

Core-shell structured BT@C hybrid particles were fabricated by CVD, and their PVDF-HFP composites were prepared by solution blend. Owing to the C-shell, BT@C hybrid particles compared with BT can effectively enhance the dielectric performance of polymer based composites. The dielectric constant of composites with 30 vol% BT@C reaches 1044 at 1 kHz and the experimental results of composites fit well with percolation theory. The existence of C-shell makes BT@C hybrid particles similar to conductive filler. The energy storage density of all composites is larger than that of pure PVDF-HFP. The relation between C-shell and dielectric properties in composites is discussed and analyzed. With the volume fraction increasing, the activation energy of composites possesses a change from positive to negative value. The existence of C-shell provides the condition for charge, which results in large interfacial polarization. The easy processibility and excellent dielectric behavior make PVDF-HFP/BT@C composites attractive as potential candidate for practical application in embedded devices and high charge-storage capacitors in the electronic industry.

Acknowledgements

This work was financially supported by the National Nature Science Foundation of China (Grant No. 11272102) and Open Project of Key Laboratory of Engineering Dielectrics and Its Application (Grant No. DJZ201401).

Notes and references

- Z. M. Dang, T. Zhou, S. H. Yao, J. K. Yuan, J. W. Zha, H. T. Song, J. Y. Li, Q. Chen, W. T. Yang and J. Bai, *Adv Mater*, 2009, **21**, 2077-2082.
- X. Huang and P. Jiang, *Adv Mater*, 2015, **27**, 546-554.
- H. X. Tang, Y. R. Lin and H. A. Sodano, *Adv Energy Mater*, 2013, **3**, 451-456.
- D. R. Wang, T. Zhou, J. W. Zha, J. Zhao, C. Y. Shi and Z. M. Dang, *J Mater Chem A*, 2013, **1**, 6162-6168.
- S. H. Yao, J. K. Yuan, T. Zhou, Z. M. Dang and J. B. Bai, *J Phys Chem C*, 2011, **115**, 20011-20017.
- P. H. Hu, Y. Shen, Y. H. Guan, X. H. Zhang, Y. H. Lin, Q. M. Zhang and C. W. Nan, *Adv Funct Mater*, 2014, **24**, 3172-3178.
- J. W. Zha, Z. M. Dang, T. Yang, T. Zhou, H. T. Song and S. T. Li, *IEEE T Dielect El In*, 2012, **19**, 1312-1317.
- M. J. Jiang, Z. M. Dang, M. Bozlar, F. Miomandre and J. B. Bai, *J Appl Phys*, 2009, **106**.
- Z. M. Dang, J. W. Zha, Y. Yu, T. Zhou, H. T. Song and S. T. Li, *IEEE T Dielect El In*, 2011, **18**, 1518-1525.
- X. Zhang, W. W. Chen, J. J. Wang, Y. Shen, L. Gu, Y. H. Lin and C. W. Nan, *Nanoscale*, 2014, **6**, 6701-6709.
- H. X. Tang, Y. R. Lin and H. A. Sodano, *Adv Energy Mater*, 2012, **2**, 469-476.
- Z. M. Dang, J. K. Yuan, J. W. Zha, T. Zhou, S. T. Li and G. H. Hu, *Prog Mater Sci*, 2012, **57**, 660-723.
- J. K. Yuan, W. L. Li, S. H. Yao, Y. Q. Lin, A. Sylvestre and J. B. Bai, *Appl Phys Lett*, 2011, **98**.
- Z. M. Dang, Y. Q. Lin, H. P. Xu, C. Y. Shi, S. T. Li and J. B. Bai, *Adv Funct Mater*, 2008, **18**, 1509-1517.
- J. J. Li, S. I. Seok, B. J. Chu, F. Dogan, Q. M. Zhang and Q. Wang, *Adv Mater*, 2009, **21**, 217-221.
- L. Qi, B. I. Lee, S. H. Chen, W. D. Samuels and G. J. Exarhos, *Adv Mater*, 2005, **17**, 1777-1781.
- Y. Feng, W. L. Li, Y. F. Hou, Y. Yu, W. P. Cao, T. D. Zhang and W. D. Fei, *J Mater Chem C*, 2015, **3**, 1250-1260.
- H. X. Tang, M. H. Malakooti and H. A. Sodano, *Appl Phys Lett*, 2013, **103**.
- S. H. Liu, J. W. Zhai, J. W. Wang, S. X. Xue and W. Q. Zhang, *ACS Appl Mater Inter*, 2014, **6**, 1533-1540.
- L. Wang and Z. M. Dang, *Appl Phys Lett*, 2005, **87**.
- C. Wu, X. Y. Huang, G. L. Wang, X. F. Wu, K. Yang, S. T. Li and P. K. Jiang, *J Mater Chem*, 2012, **22**, 7010-7019.
- Z. M. Dang, Y. Shen and C. W. Nan, *Appl Phys Lett*, 2002, **81**, 4814-4816.
- Y. Deng, Y. J. Zhang, Y. Xiang, G. S. Wang and H. B. Xu, *J Mater Chem*, 2009, **19**, 2058-2061.
- Y. Li, X. Y. Huang, Z. W. Hu, P. K. Jiang, S. T. Li and T. Tanaka, *ACS Appl Mater Inter*, 2011, **3**, 4396-4403.
- S. H. Yao, Z. M. Dang, M. J. Jiang and J. B. Bai, *Appl Phys Lett*, 2008, **93**.
- B. S. Prakash and K. B. R. Varma, *Compos Sci Technol*, 2007, **67**, 2363-2368.
- A. B. Dichiaro, J. K. Yuan, S. H. Yao, A. Sylvestre, L. Zimmer and J. B. Bai, *J Mater Chem A*, 2014, **2**, 7980-7987.
- Q. Li, Q. Z. Xue, L. Z. Hao, X. L. Gao and Q. B. Zheng, *Compos Sci Technol*, 2008, **68**, 2290-2296.
- Q. K. Guo, Q. Z. Xue, J. Sun, M. D. Dong, F. J. Xia and Z. Y. Zhang, *Nanoscale*, 2015, **7**, 3660-3667.
- X. Y. Huang, L. Y. Xie, K. Yang, C. Wu, P. K. Jiang, S. T. Li, S. Wu, K. Tatsumi and T. Tanaka, *IEEE T Dielect El In*, 2014, **21**, 467-479.
- X. H. Zhang, Y. H. Ma, C. W. Zhao and W. T. Yang, *Appl Surf Sci*, 2014, **305**, 531-538.

32. T. Zhou, J. W. Zha, Y. Hou, D. R. Wang, J. Zhao and Z. M. Dang, *ACS Appl Mater Inter*, 2011, **3**, 4557-4560.
33. Z. D. Liu, Y. Feng and W. L. Li, *RSC Adv*, 2015, **5**, 29017-29021.
34. S. B. Luo, S. H. Yu, R. Sun and C. P. Wong, *ACS Appl Mater Inter*, 2014, **6**, 176-182.
35. Y. Yang, H. L. Sun, D. Yin, Z. H. Lu, J. H. Wei, R. Xiong, J. Shi, Z. Y. Wang, Z. Y. Liu and Q. Q. Lei, *J Mater Chem A*, 2015, **3**, 4916-4921.
36. L. Huang, P. L. Zhu, G. Li, D. Q. Lu, R. Sun and C. P. Wong, *J Mater Chem A*, 2014, **2**, 18246-18255.
37. M. Meyyappan, L. Delzeit, A. Cassell and D. Hash, *Plasma Sources Sci T*, 2003, **12**, 205-216.
38. Y. C. Choi, Y. M. Shin, S. C. Lim, D. J. Bae, Y. H. Lee, B. S. Lee and D. C. Chung, *J Appl Phys*, 2000, **88**, 4898-4903.
39. K. C. Huang, T. C. Huang and W. F. Hsieh, *Inorg Chem*, 2009, **48**, 9180-9184.
40. K. N. Kudin, B. Ozbas, H. C. Schniepp, R. K. Prud'homme, I. A. Aksay and R. Car, *Nano Lett*, 2008, **8**, 36-41.
41. D. Y. Wan, C. Y. Yang, T. Q. Lin, Y. F. Tang, M. Zhou, Y. J. Zhong, F. Q. Huang and J. H. Lin, *ACS Nano*, 2012, **6**, 9068-9078.
42. Y. Q. Lin, A. Dichiaro, D. L. He, P. Haghi-Ashtiani and J. B. Bai, *Chem Phys Lett*, 2012, **554**, 137-142.
43. T. Sharifi, F. Nitze, H. R. Barzegar, C. W. Tai, M. Mazurkiewicz, A. Malolepszy, L. Stobinski and T. Wagberg, *Carbon*, 2012, **50**, 3535-3541.
44. C. Singh, M. S. Shaffer and A. H. Windle, *Carbon*, 2003, **41**, 359-368.
45. H. K. Jeong, Y. P. Lee, M. H. Jin, E. S. Kim, J. J. Bae and Y. H. Lee, *Chem Phys Lett*, 2009, **470**, 255-258.
46. W. Z. Ma, J. Zhang and X. L. Wang, *Appl Surf Sci*, 2008, **254**, 2947-2954.
47. M. C. Araujo, C. M. Costa and S. Lanceros-Mendez, *J Non-Cryst Solids*, 2014, **387**, 6-15.
48. C. W. Nan, Y. Shen and J. Ma, *Annu Rev Mater Res*, 2010, **40**, 131-151.
49. J. C. Dyre and T. B. Schroder, *Rev Mod Phys*, 2000, **72**, 873-892.
50. F. He, S. Lau, H. L. Chan and J. T. Fan, *Adv Mater*, 2009, **21**, 710-715.
51. Y. J. Li, M. Xu, J. Q. Feng and Z. M. Dang, *Appl Phys Lett*, 2006, **89**.
52. Z. M. Dang, S. H. Yao, J. K. Yuan and J. B. Bai, *J Phys Chem C*, 2010, **114**, 13204-13209.
53. Z. M. Dang, J. K. Yuan, S. H. Yao and R. J. Liao, *Adv Mater*, 2013, **25**, 6334-6365.
54. T. Tanaka, *IEEE T Dielect El In*, 2005, **12**, 914-928.
55. R. C. Smith, C. Liang, M. Landry, J. K. Nelson and L. S. Schadler, *IEEE T Dielect El In*, 2008, **15**, 187-196.
56. Q. G. Chi, J. Sun, C. H. Zhang, G. Liu, J. Q. Lin, Y. N. Wang, X. Wang and Q. Q. Lei, *J Mater Chem C*, 2014, **2**, 172-177.
57. W. H. Yang, S. H. Yu, R. Sun and R. X. Du, *Acta Mater*, 2011, **59**, 5593-5602.
58. J. I. Hong, L. S. Schadler, R. W. Siegel and E. Martensson, *Appl Phys Lett*, 2003, **82**, 1956-1958.

Graphical Abstract

Core-shell structured BaTiO_3 @Carbon hybrid particles fabricated via chemical vapor deposition can remarkably enhance the dielectric performance of polymer composites.

